A small-molecule scaffold induces autophagy in primary neurons and protects against toxicity in a Huntington disease model

Andrey S. Tsvetkov[a], Jason Miller[a,b,c], Montserrat Arrasate[a], Jinny S. Wong[a], Michael A. Pleiss[a], and Steven Finkbeiner[a,d,e,f,g,1]

[a]Gladstone Institute of Neurological Disease and the Taube–Koret Center for Huntington's Disease Research and the Consortium for Fronto-temporal Dementia Research, University of California, San Francisco, CA 94158; and [b]Chemistry and Chemical Biology Program, [c]Medical Scientist Training Program, [d]Neuroscience Program, [e]Biomedical Sciences Program, and Departments of [f]Neurology and [g]Physiology, University of California, San Francisco, CA 94143

Edited by Solomon H. Snyder, The Johns Hopkins University School of Medicine, Baltimore, MD, and approved August 17, 2010 (received for review April 2, 2010)

Autophagy is an intracellular turnover pathway. It has special relevance for neurodegenerative proteinopathies, such as Alzheimer disease, Parkinson disease, and Huntington disease (HD), which are characterized by the accumulation of misfolded proteins. Although induction of autophagy enhances clearance of misfolded protein and has therefore been suggested as a therapy for proteinopathies, neurons appear to be less responsive to classic autophagy inducers than nonneuronal cells. Searching for improved inducers of neuronal autophagy, we discovered an N^{10}-substituted phenoxazine that, at proper doses, potently and safely up-regulated autophagy in neurons in an Akt- and mTOR-independent fashion. In a neuron model of HD, this compound was neuroprotective and decreased the accumulation of diffuse and aggregated misfolded protein. A structure/activity analysis with structurally similar compounds approved by the US Food and Drug Administration revealed a defined pharmacophore for inducing neuronal autophagy. This pharmacophore should prove useful in studying autophagy in neurons and in developing therapies for neurodegenerative proteinopathies.

Akt | light-chain 3 | neuronal autophagy | phenoxazine

Macroautophagy (hereafter referred to as autophagy) is used by cells to remove long-lived proteins, organelles, or parasites (1) and involves sequestration of material inside double-membrane vesicles called autophagosomes, which fuse to lysosomes to degrade vesicle contents for reuse in cellular processes. Autophagy is important in neuronal survival: Mice deficient in autophagy develop neurodegeneration (2). Deficient autophagy might allow accumulation of misfolded proteins that lead to neurodegenerative proteinopathies (3). In cell lines, clearance of mutated α-synuclein, implicated in Parkinson disease, depends on autophagy (4). Other examples of autophagy's involvement in neurodegeneration are amyotrophic lateral sclerosis (5), Huntington disease (HD) (6), and Alzheimer disease (7).

Studies in cell lines and fly models of neurodegenerative diseases suggest that autophagy can be enhanced to remove misfolded proteins and might be therapeutical (1). One of the best-studied pharmacological inducers of autophagy is rapamycin, which inhibits mTOR, a key regulator of cell growth and proliferation. In cell line and fly models, rapamycin slows accumulation of misfolded proteins implicated in several neurodegenerative diseases (1). In a mouse model of HD, everolimus, a rapamycin analogue, induced autophagy in muscle but not in brain (8). Compounds that decrease inositol levels also induce autophagy (5, 9). Screens for small-molecule enhancers of autophagy in nonneuronal cells yielded a diverse set of structurally unrelated autophagy activators, some of which might act via similar pathways (9–11).

Autophagy stimulators have been studied mainly in nonneuronal cells and cell lines. However, autophagy might be regulated differently in primary neurons and other cell types (12). Chemical inhibition of the proteasome affects lipidated light-chain 3 (LC3-II) levels much less in primary neurons than in nonneuronal cells (13, 14). Starvation, the best-known inducer of autophagy in most nonneuronal cells, does not induce autophagy in the cortices of mice (15). mTOR activity is not affected in most parts of the starving brain (16). Rapamycin weakly induces autophagy in cortical neurons, causing atypical features of autophagy (17). Protective properties of rapamycin might also arise from pathways that are not related to autophagy (18, 19). Discovery of safe and effective autophagy inducers in neurons would be highly desirable.

Because autophagy induction may differ in neurons and nonneuronal cells (12), we searched for small molecules that induce autophagy in neurons. We discovered a class of structurally related compounds, most of which are approved for human use, that induce autophagy in primary neurons and protect against degeneration in a neuron model of HD.

Results

N^{10}-Substituted Phenoxazine Induces Neuronal Autophagy. Inhibiting mTOR with rapamycin induces autophagy strongly in nonneuronal cells but weakly in neurons (17), suggesting underlying differences in the mTOR complex. We tested whether autophagy could be activated in neurons by targeting a major upstream mTOR regulator kinase, Akt. We incubated neurons with the Akt inhibitor, 10-[4′-(*N*-diethylamino)butyl]-2-chlorophenoxazine (10-NCP) (20).

When autophagy is active in cells, the autophagy-related protein LC3 is lipidated. Conversion from nonlipidated LC3 (LC3-I) to lipidated LC3 (LC3-II), detected as a mobility shift in Western blot analyses (21, 22), was induced more strongly in primary neurons by 10-NCP (Fig. 1 *A–C*) than by rapamycin or everolimus, its more stable analogue (Fig. S1). Our results are consistent with those observed by others: If rapamycin induces autophagy in neurons, it does so weakly (8, 17). Indeed, it was suggested that rapamycin inhibits polyglutamine protein aggregation independent of autophagy (19).

Increased LC3-II levels could result from autophagy or blockade at some step after the conversion of LC3-I to LC3-II. To address this, we incubated primary striatal neurons with 10-NCP and bafilomycin A, which inhibits the last step of autophagy-mediated degradation (23). LC3-II levels were higher in neurons treated with the combination of drugs than in neurons treated only with 10-NCP (Fig. 1*D*), indicating that 10-NCP induces autophagy.

Author contributions: A.S.T., J.M., M.A., and S.F. designed research; A.S.T., M.A., and J.S.W. performed research; A.S.T., J.S.W., and M.A.P. analyzed data; and A.S.T., J.M., M.A.P., and S.F. wrote the paper.

The authors declare no conflict of interest.

This article is a PNAS Direct Submission.

[1]To whom correspondence should be addressed. E-mail: sfinkbeiner@gladstone.ucsf.edu.

This article contains supporting information online at www.pnas.org/lookup/suppl/doi:10.1073/pnas.1004498107/-/DCSupplemental.

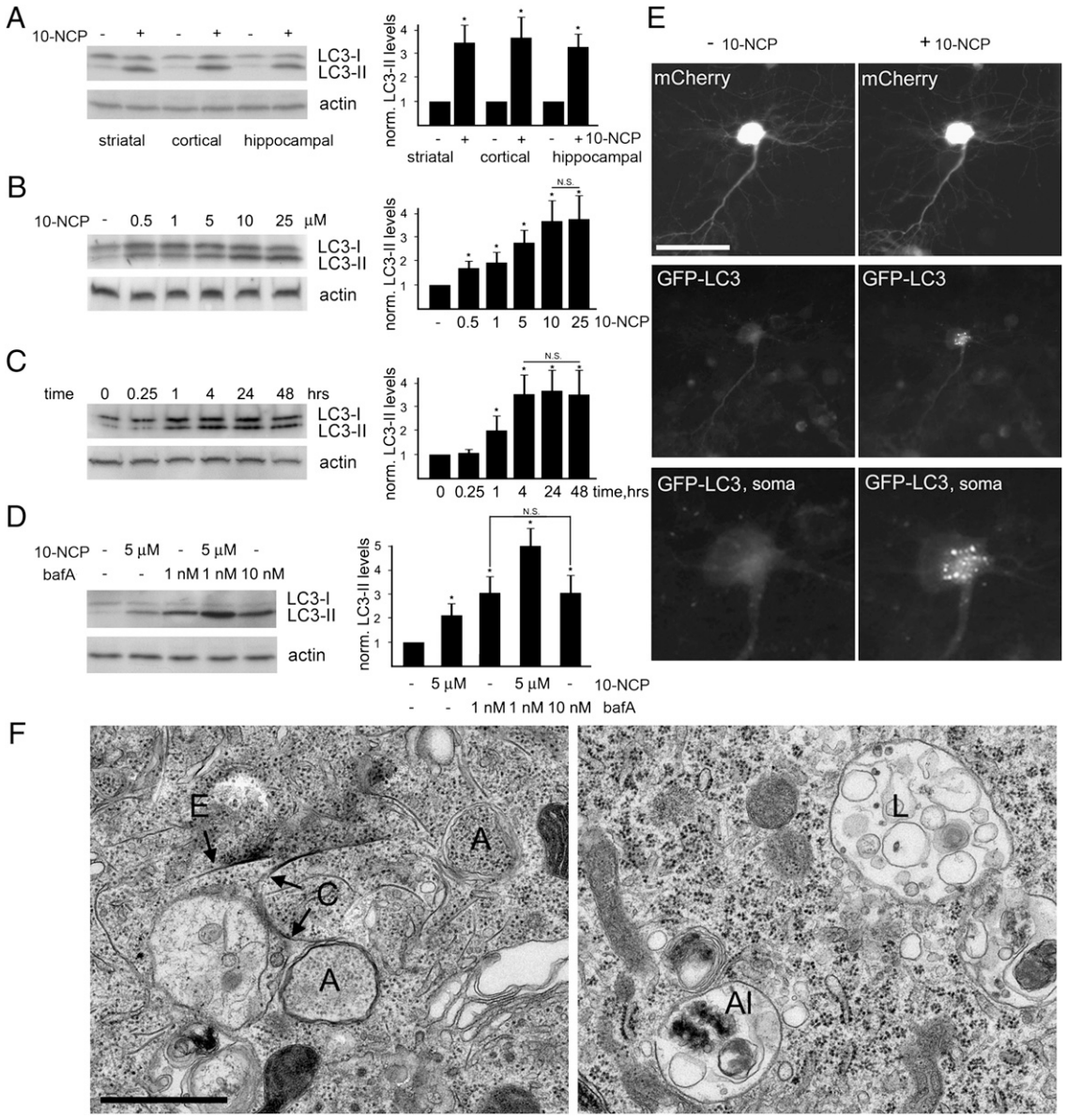

Fig. 1. N^{10}-substituted phenoxazine (10-NCP) induces autophagy in primary neurons. (*A*) Autophagy was efficiently induced in striatal, cortical, and hippocampal neurons by 10 μM 10-NCP as reflected by the increased levels of LC3-II. Actin was used as a loading control throughout this figure. $*P < 0.001$ (pairwise *t* test). norm., normalized. (*B*) Autophagy was efficiently induced in striatal neurons by 0.5, 1, 5, 10, and 25 μM 10-NCP (overnight). $*P < 0.01$ (ANOVA). The slight increase in LC3-I levels represents up-regulation of the LC3 gene. N.S., not significant. (*C*) LC3-II accumulation is noticeable 1 h after treatment with 10 μM 10-NCP. LC3-II levels peak at ~4 h in cultured striatal neurons. $*P < 0.01$ (ANOVA). (*D*) LC3-II accumulation in striatal neurons treated with 5 μM 10-NCP with or without 1 nM bafilomycin A (10-NCP, overnight; bafilomycin A was then added for 4 h). Bafilomycin A reached a ceiling effect, and higher concentrations (e.g., 10 nM) did not further increase LC3-II levels. LC3-II increased in 10-NCP–treated cells when bafilomycin A was added. The film was exposed to encompass all signals fully but especially to demonstrate the differences in LC3-II levels. $*P < 0.001$ (ANOVA). (*E*) Striatal neuron from GFP-LC3 transgenic mice expressing mCherry before (*Left*) and after (*Right*) treatment with 10-NCP (10 μM, 4 h). Note the changes in GFP-LC3 localization, which were consistent with GFP-LC3 relocalization to autophagosomes. (Scale bar, 50 μm.) (*F*) Electron micrographs of striatal neurons treated with 10-NCP (10 μM, overnight) (0- and 1-μM conditions are shown in Fig. S2). A, autophagosomes; Al, autolysosome; C, curving phagophores; E, extending phagophore; L, lysosome with degraded contents. (Scale bar, 0.6 μm.) Quantification of autophagic structures in neurons treated with 0, 1, and 10 μM 10-NCP is shown in Fig. S2.

If 10-NCP increases LC3-II levels by promoting autophagy, it should induce formation of GFP-LC3-positive autophagosomes in GFP-LC3 transgenic neurons (15). To score autophagy induction from fluorescence images, we measured the redistribution of GFP-LC3 into autophagosomes, as reflected by the puncta index—the SD among pixels within the cellular region of interest—before and after treatment. Diffuse localization corresponds to a low puncta index, and punctate localization corresponds to a high puncta index (24). In live striatal neurons from GFP-LC3 mice, even a short incubation (4 h) with 10-NCP produced GFP-LC3-positive puncta (Fig. 1*E*). The puncta index was significantly higher after the treatment (430 ± 60 vs. 1,210 ± 300; $P < 0.001$).

To confirm that 10-NCP–treated neurons form autophagosomes and phagophores, we examined cells by electron microscopy (25). Autophagosomes were rare in control cells, and no phagophores were observed, presumably reflecting their transience (Fig. S2). However, neurons treated with 10-NCP had dose-dependent increases in autophagosomes and autolysosomes (Fig. 1*F* and Fig. S2) and contained multilamellar vesicular structures implicated in autophagy (26) that were rare in untreated cells (Fig. S2). All these

structures were observed in neuronal somas and nerve terminals. Extending and curving phagophores (26) were also more frequent in treated neurons (Fig. 1*F*). The increase in autophagosome precursors (Fig. 1*F*) rather than in autophagosomes per se suggests that NCP-10 induces neuronal autophagy.

10-NCP Up-Regulates Autophagy in Neurons Without Overt Toxicity and Is Protective in a Primary Neuron Model of HD. To determine if 10-NCP safely induces sustained autophagy in neurons, we treated primary striatal neurons with 1 or 10 μM 10-NCP or vehicle and calculated the cumulative risk for death with automated microscopy and longitudinal analysis (27, 28). Neurons were transfected with GFP, drug or vehicle was added, and hundreds of transfected neurons were individually tracked for 7 d. Loss of GFP is a highly sensitive marker for neuronal death (27, 28). By monitoring when each neuron lost its GFP fluorescence, we could analyze neuronal death with cumulative hazard statistics. Treatment with 1 μM 10-NCP moderately induced LC3-II levels (Fig. 1*B*) and improved survival (Fig. 2*A*). Treatment with 10 μM more strongly induced LC3-II levels (Fig. 1*B*) but was toxic (Fig. 2*A*).

We hypothesized that 1 μM 10-NCP might be protective in a primary neuron model of HD (13, 27, 28), a neurodegenerative proteinopathy caused by an abnormal polyglutamine expansion in huntingtin (Htt). This expansion triggers toxicity and aggregation of Htt into inclusion bodies (IBs). Striatal neurons were transfected with mCherry (a morphology and viability marker) and an amino-terminal exon 1 fragment of mutant Htt (Htt^{ex1}) containing a pathogenic stretch of 72 glutamines fused to the N terminus of GFP. One day after transfection, neurons were treated with vehicle or 1 μM 10-NCP and individually monitored every 24 h with our automated microscope for loss of the mCherry survival marker. Kaplan–Meier and cumulative hazard plots of these data revealed that neurons expressing mutant Htt that were treated with 10-NCP survived better than vehicle-treated neurons (Fig. 2*B*).

If this protective effect is principally mediated by enhanced autophagic turnover of mutant Htt, steady-state levels of mutant Htt in treated neurons should decrease, resulting in fewer IBs and less diffuse mutant Htt (27). In a small percentage of untreated neurons, IBs spontaneously disappeared (Fig. 2 *C* and *D*) and the neuron remained alive, suggesting that neurons have mechanisms, possibly involving autophagy, to clear these structures that and 10-NCP might stimulate basal autophagy. The rate of IB disappearance was higher in treated than in untreated neurons (Fig. 2*C*), and clearance of mutant Htt was associated with reversal of the neurite retraction seen in many mutant Htt-expressing neurons (Fig. S3). However, in neurons treated with bafilomycin A, which inhibits productive autophagy, the rate of IB clearance fell (Fig. 2*C*).

10-NCP also reduced the fraction of neurons with IBs and the risk of IB formation (Fig. 2 *E* and *F*); in addition, it reduced levels of diffuse mutant Htt (Fig. 2*G*), even when the initial expression was similar to that of endogenous Htt (*Materials and Methods*). In cultured primary neurons from R6/2 HD mice (29), 10-NCP lowered mutant protein levels (Fig. S4). Thus, 10-NCP might have therapeutical benefit in HD and other neurodegenerative diseases by enhancing autophagic turnover of mutant protein.

10-NCP Up-Regulates Autophagy in Neurons in an Akt- and mTOR-Independent Fashion. To test whether 10-NCP's ability to induce autophagy in neurons is attributable to its ability to inhibit Akt, we evaluated structurally unrelated compounds V, VII, and IX, which inhibit Akt activity by different putative mechanisms (20, 30). All inhibited Akt, but none induced neuronal autophagy (Fig. S5*A*). This suggests that 10-NCP induces autophagy through an Akt-independent mechanism (Fig. S5*B*). Indeed, in primary neurons, 10-NCP induced autophagy without stimulating the activating phosphorylations of mTOR or p70S6K, which are kinases downstream of Akt activation (Fig. S5*B*).

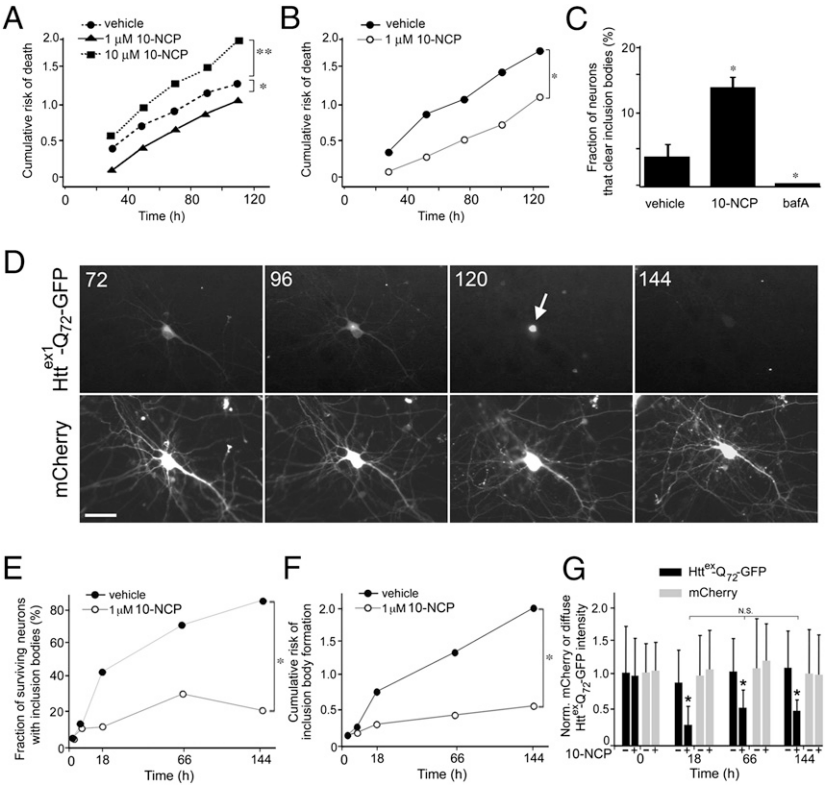

Fig. 2. 10-NCP is not toxic to neurons, decreases diffuse and aggregated forms of mutant Htt^{ex1} protein, and is protective in a neuron model of HD. (*A*) Cumulative risk for death associated with 10-NCP treatment of GFP-transfected striatal neurons. Treatment with low-dose (1 μM, weak stimulation of autophagy) 10-NCP led to a small decrease in baseline risk for death. A higher dose (10 μM, overstimulated autophagy) led to increased cell death. Note differences in LC3-II levels in neurons treated with 1 and 10 μM 10-NCP in Fig. 1*B*. $*P < 0.001$; $**P < 0.0001$ (Mantel–Cox test). (*B*) Striatal neurons transfected with mCherry and mutant Htt^{ex1}-GFP were treated with 1 μM 10-NCP or vehicle. Cumulative risk for death was calculated from Kaplan–Meier curves. 10-NCP reduced the risk for death (i.e., improved survival) of neurons expressing mutant Htt^{ex1}. $*P < 0.001$ (Mantel–Cox test). (*C*) Fraction of neurons that formed IBs and subsequently cleared IBs in the presence of vehicle, 1 μM 10-NCP, and 1 nM bafilomycin A (bafA). Neurons were transfected as in *B* and were followed with an automated microscope for several days. $*P < 0.001$ (ANOVA). (*D*) IB (arrow) that spontaneously disappeared during the experiments in *C*. Numbers reflect hours after transfection (Fig. S3). (Scale bar, 15 μm.) (*E*) Two cohorts of neurons transfected and treated as in *A* were monitored longitudinally. The fraction of surviving neurons with IBs was greater after treatment with vehicle than with 10-NCP. $*P < 0.001$ (*t* test). (*F*) Cumulative risk for IB formation in neurons transfected and treated as in *A* shows that IBs form more readily in untreated neurons. $*P < 0.0001$ (Mantel–Cox test). (*G*) Levels of diffuse mutant Htt and mCherry from neurons transfected and treated as in *B*. After exclusion of neurons with IBs, GFP or mCherry levels were normalized (Norm.) to fluorescence at the first time point. The levels of cotransfected mCherry did not change. $*P < 0.01$ (ANOVA). N.S., not significant.

US Food and Drug Administration-Approved Structurally Related Analogues of 10-NCP Induce a Protective Neuronal Autophagy Response. Next, we wondered whether structural analogues of 10-NCP would also induce neuronal autophagy, thereby suggesting a defined structure/activity relationship. Several US Food and Drug Administration (FDA)-approved compounds in different classes of the tricyclics (trifluoperazine, promazine and its analogues, promethazine, thioridazine, and mesoridazine) induced neuronal autophagy (Fig. 3 and Fig. S6); only trifluoperazine was known to enhance autophagy (10). Nonsubstituted phenoxazine and phenothiazine did not stimulate autophagy, suggesting that an amino-containing substituent at the N^{10} position is important for activity.

We also tested nortriptyline, another tricyclic compound (Fig. 3), with a secondary amine originating from the analogous central ring position of the phenothiazine compounds. Notably, however, the central ring of nortriptyline lacks heteroatoms. Overnight incubation with nortriptyline induced neuronal autophagy (Fig. S6).

Quinacrine has a tricyclic acridine ring structure with an aliphatic tertiary amine substituent originating from the central ring (Fig. 3). Surprisingly, quinacrine did not induce autophagy (Fig. 3 and Fig. S6). Structurally, quinacrine differs in two major ways from the other tricyclic drugs that induce autophagy. It contains a 4-aminopyridine central ring, which adds significant polarity to the ring structure, and its tricyclic ring is strictly planar (the other tricyclics are less rigid). One or both of these differences might explain quinacrine's inability to induce autophagy.

With an understanding of the structure/function relationship between aliphatic amino-substituted tricyclic compounds and neuronal autophagy induction, we searched for our newly defined structural scaffold among the top hits from another screen for autophagy inducers in a glioblastoma cell line (10). Four of the eight top hits had previously unrecognized structural similarities to our tricyclic autophagy inducers (with an additional hit being trifluoperazine). These compounds (i.e., niguldipine, pimozide, fluspirilene, loperamide) contain a biphenyl core and a 3–4 carbon linker to a tertiary amine. This related structural scaffold induced autophagy in primary neurons (Fig. 3 and Fig. S6).

To confirm the generalizability of the scaffold as a therapeutical lead, we established that nortriptyline is neuroprotective in our primary striatal culture model of HD (Fig. S7).

Compounds That Induce Autophagy in Neurons Can Be Fitted to a Multifeatured Pharmacophore. Rank ordering of the autophagy-inducing potencies of the compounds (Fig. 3) suggested several chemical features of our putative scaffold that might be important for activity. To assemble these features into a more refined pharmacophore, we applied the HipHop algorithm (31) in the Pharmacophore Protocol within Discovery Studio version 2 (Accelrys) to the two most active autophagy-inducing compounds, 10-NCP and trifluoperazine. This algorithm evaluates hydrophobic, aromatic, acceptor, donor, and charged chemical features that the two compounds have in common based on shared conformations. Up to 255 low-energy conformations of each compound were included in the analysis. The algorithm starts by matching a small set of features and then searches for more shared features until no further common conformation of the input compounds is found. Multiple hypotheses involving the spatial orientation of shared chemical features between the input compounds were generated and scored. All hypotheses with three or four shared chemical features were evaluated with the Ligand Pharmacophore Mapping function and scoring module in the Pharmacophore Protocol of Discovery Studio and used to fit the remaining compounds in Fig. 3.

Drug	Structure	Neuronal autophagy stimulation
10-NCP	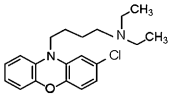	+ + + + +
Trifluoperazine	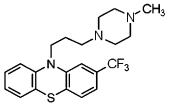	+ + + + +
Promazine Chlorpromazine Triflupromazine	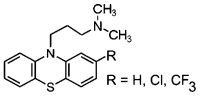	+ + + +
Promethazine	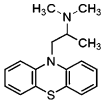	+ + + +
Mesoridazine	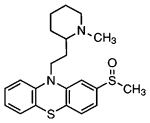	+ + +
Thioridazine	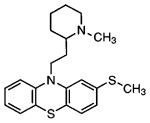	+ + +
Nortriptyline	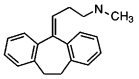	+

Drug	Structure	Neuronal autophagy stimulation
Phenoxazine	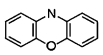	-
Phenothiazine	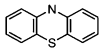	-
Quinacrine	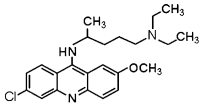	-
Niguldipine	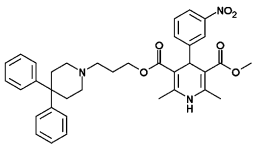	+ +
Loperamide	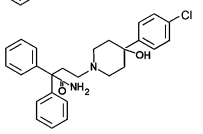	+ +
Pimozide	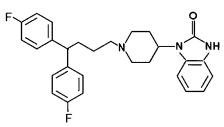	+ +
Fluspirilene	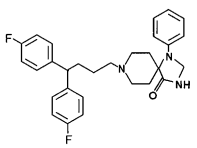	+ +

Fig. 3. Structural scaffold that induces neuronal autophagy. Chemical structures of compounds that induced autophagy in striatal, cortical, and hippocampal neurons. Note the base ring structure (or a biphenyl ring system for pimozide, niguldipine, loperamide, and fluspirilene) with a 2–5 carbon aliphatic substituent linker that contains a secondary or tertiary amine. Phenoxazine, phenothiazine, and quinacrine failed to induce autophagy and variably lacked the amino-capped substituent, had a 4-aminopyridine central ring, or had a strictly planar tricyclic ring system. Potency of the drugs was assayed in striatal neurons using the levels of LC3-II induction for each compound at 0.5, 1, and 5 μM as a semiquantitative readout (Fig. S6). Ranked potencies fell into five groups: +++++, 10-NCP and trifluoperazine (strongest stimulators); ++++, promazine, promethazine, chlorpromazine, and triflupromazine; +++, mesoridazine and thioridazine (medium stimulators); ++, niguldipine, loperamide, pimozide, and fluspirilene; +, nortriptyline (weakest stimulator). –, Drugs that do not induce autophagy.

None of the initial three- or four-feature models explained the potencies of all compounds in Fig. 3. Therefore, the most promising three-feature pharmacophore model (two hydrophobic aromatic features and one charged positive feature) was selected and modified to contain areas of ligand inaccessibility (exclusion spheres). Systematic incorporation of 14 exclusion spheres eventually led to the proper potency ranking of all compounds. The pharmacophore model with three positive features fitted to trifluoperazine is shown in Fig. S8*A*. The same model was fitted to trifluoperazine but with 14 exclusion spheres (Fig. S8*B*). The best low-energy conformations of trifluoperazine and 10-NCP were superimposed (Fig. S8*C*). Both fit the model well, but the chlorine of 10-NCP occupied a different space relative to the trifluoromethyl moiety of trifluoperazine. Because the chlorine and trifluoromethyl moieties are both hydrophobic and electron-withdrawing, it is unclear whether either property was important for activity.

Analysis of less active compounds revealed more interesting features of the refined pharmacophore model. For example, pimozide's best fit involves only one of the 4-fluoro-phenyl groups; the second occupies a region outside the three-feature pharmacophore model and away from any exclusion sphere of the model. Pimozide's conformation allows its amine to fit into the charged positive feature of the pharmacophore model (Fig. S8*D*). The second hydrophobic aromatic fit of pimozide into the pharmacophore model is made partially by the benzimidazole-2-one moiety. This fit is not ideal, which probably accounts for pimozide's moderate activity (Fig. 3 and Fig. S6). Pimozide therefore shows the importance of nonobvious and discontinuous features (e.g., benzimidazole-2-one moiety) in satisfying a complex pharmacophore model.

Discussion

We sought improved inducers of autophagy specifically for a primary neuronal system (13, 27, 28). Previous studies suggested that autophagy might be induced differently in neurons and nonneuronal cells (12–14). Indeed, inhibition of mTOR with rapamycin and its analogue, everolimus, strongly induced autophagy in a nonneuronal cell line but very weakly, if at all, in neurons. A similar result was observed in a mouse model of HD (8). Because autophagy induction and the resulting turnover of misfolded toxic proteins have been proposed as a neuroprotective strategy for many neurodegenerative diseases, our quest for strong autophagy inducers in neurons has therapeutical implications.

We started our search with 10-NCP and discovered its ability to induce autophagy safely in striatal, cortical, and hippocampal neurons. At 1 μM, 10-NCP protected against mutant Htt toxicity in a primary culture model of HD and decreased diffuse and aggregated forms of mutant Htt.

Although 10-NCP inhibits Akt (20), several structurally unrelated Akt inhibitors did not induce neuronal autophagy, suggesting that 10-NCP induces autophagy through an Akt-independent mechanism. Indeed, 10-NCP did not change the activation status of two kinases downstream of Akt, mTOR and p70S6K in primary neurons. Because 10-NCP inhibits Akt by competing with ATP for binding to the kinase (20), the compound's autophagy-inducing effects might instead derive from inhibiting a different kinase ATP-binding pocket.

To explore the structure/function relationship between 10-NCP and autophagy induction further, we tested a series of structurally related phenothiazine and phenoxazine derivatives. Compounds with a 2–5 carbon aliphatic substituent originating from the central ring and capped by an amine induced autophagy, but unsubstituted phenoxazine and phenothiazine did not. Nortriptyline also induced autophagy, suggesting that the phenothiazine or phenoxazine tricyclic scaffold is not absolutely necessary for activity. However, quinacrine failed to induce autophagy. We suspect that quinacrine's 4-aminopyridine central ring or its strictly planar tricyclic ring system plays a role in abrogating autophagy induction.

We found that niguldipine, pimozide, fluspirilene, and loperamide, which were identified in a previous screen for autophagy inducers in a glioblastoma cell line (10), had unrecognized structural similarities to the tricyclic and aliphatic amine substituent scaffold we identified as critical for autophagy induction in neurons. These compounds have a biphenyl core and a 3–4 carbon linker to a tertiary amine. This structural scaffold also induced autophagy in our primary neuronal system. Interestingly, pimozide, niguldipine, loperamide, and fluspirilene, like 10-NCP, induce autophagy without altering mTOR activation (10). This observation suggests this structural class of autophagy inducers acts through a mechanism distinct from rapamycin's induction of autophagy.

To refine further the explanatory model for the ranked potencies of all autophagy-inducing compounds that we tested, we built a multifeatured pharmacophore. The pharmacophore suggests future avenues for structure/activity analysis, including the planarity, heteroatom composition, and charge of the ring system; the length, substitution pattern, and rigidity of the aliphatic amine linker; and the pKb and steric bulkiness of the terminal amine on the linker.

In initial tests of 10-NCP, we were concerned about its therapeutical potential because it apparently inhibits Akt (Fig. S5*A*), a survival factor for neurons (28). Several factors argue against this concern. First, 10-NCP safely up-regulated autophagy in primary neurons and was neuroprotective in a primary neuronal HD model. Second, although the compound appeared to reduce Akt activation in neurons, it did not affect the activation status of kinases downstream of Akt, suggesting an incomplete Akt inhibitory capacity. Third, nortriptyline, another compound from the autophagy-inducing scaffold we defined, was neuroprotective in our primary neuronal HD model even though it was not known to inhibit Akt. As we use the refined pharmacophore to screen for more compounds that may induce neuronal autophagy, we will likely encounter compounds that potently induce autophagy without affecting Akt.

The discovery of a defined small-molecule pharmacophore that reliably induces autophagy in primary neurons will facilitate the study of autophagy in neurodegenerative proteinopathies. 10-NCP appears to be safe at low doses and protective in a neuron model of HD. Importantly, many of the compounds in this autophagy-inducing structural scaffold are already FDA-approved and have no known inhibitory effects on Akt. Thus, this scaffold may serve as a pharmacophore for therapy development in neurodegenerative diseases in which protein misfolding is prominent.

Materials and Methods

Detailed methods are available in *SI Materials and Methods*.

Plasmids and Chemicals. Bafilomycin A, rapamycin, trifluoroperazine, promazine, triflupromazine, chlorpromazine, mesoridazine, promethazine, nortriptyline, phenoxazine, phenothiazine, quinacrine, loperamide, pimozide, niguldipine, fluspirilene, and actin antibody were from Sigma. Everolimus was from Walter Schuler (Novartis; Basel, Switzerland). Thioridazine was from MP Biomedicals. Akt inhibitors V, VII, IX, and 10-NCP were from Calbiochem. Previously described antibodies against LC3 (33) were from Dr. Debnath (University of California, San Francisco), or from MBL International and were then developed in our laboratory. Antibodies against Akt, phospho-Akt (Ser473), mTOR, phosphomTOR (Ser2448), p70S6K, and phospho-p70S6K (Thr389) were from Cell Signaling. Antibody 3B5H10 was from Sigma. BDNF was from Amgen. mCherry, a gift from R. Tsien (University of California, San Diego), was cloned into the pGW1 vector. pGW1-GFP and pGW1-Httex1-Q72-GFP were as described by Arrasate et al. (27).

Cell Cultures. Striata, cortices, and hippocampi from rat embryos (embryo days 17–18) or newborn (postnatal day 0) mice were dissected, dissociated, and

plated on 24-well tissue culture plates coated with poly-D-lysine, as described (27, 28, 33). Cells were cultured for 7–10 d in neurobasal medium with L-glutamine and B-27 before use.

Microscopy and Survival Analysis. Statistical analysis used Metamorph (Molecular Devices, CA), as described (27, 28), with cumulative hazard curves generated by Statview (Apple, CA). Striatal neurons expressing mutant Htt were transfected 5–7 d in vitro with pGW1-GFP (survival marker) or both pGW1-mCherry and pGW1-Htt^{ex1}-Q72-GFP at a 1:1 molar ratio (2–3 μg of total DNA in each well of a 24-well plate). Neurons were treated with vehicle (DMSO) or with 1 or 10 μM 10-NCP 24 h after transfection and imaged immediately and then every 24 h for 1 wk. Fresh 10-NCP or DMSO was provided daily by changing the medium. Neurons that died during the imaging interval were assigned a survival time (the period between transfection and their disappearance from an image). These event times were used to obtain the cumulative risk for death graph, which was analyzed for statistical significance using the Mantel–Cox test. Experiments were repeated two to three times with more than 100 neurons per condition.

Image Analysis. Measurements of Htt expression and IB formation were extracted from files obtained by automated imaging. Expression of GFP-tagged Htt was estimated by measuring GFP fluorescence intensity over a region of interest corresponding to the neuronal soma (using the fluorescence of cotransfected mCherry as a guide to draw the region of interest). The intensity values were background-subtracted and normalized to those at time "zero." To control for potential changes in transcription or translation, the intensity of mCherry, which is expressed from the same plasmid as GFP-tagged Htt, was also measured. The cumulative risk of IB formation in cohorts of neurons that asynchronously formed IBs was calculated with Statview. The time of IB formation after transfection was used as the event time variable.

Pharmacophore Modeling. Pharmacophore modeling was performed with the Pharmacophore Protocol within Discovery Studio version 2.1. Low-energy conformations of all the compounds reported in Fig. 3 were determined with the CHARMm force field within Discovery Studio version 2.1 using the default potentials.

ACKNOWLEDGMENTS. We thank Drs. N. Mizushima (Tokyo Medical and Dental University, Japan) and Riken BRC (Japan) for GFP-LC3 mice, R. Tsien (University of California, San Diego) for mCherry, and J. Debnath (University of California, San Francisco) for LC3 antibodies and helpful discussions. We thank Dr. Walter Schuler (Novartis) for everolimus and helpful discussions. We also thank Dr. A.M. Cuervo and members of the Finkbeiner laboratory for helpful discussions. K. Nelson provided administrative assistance, and G. Howard and S. Ordway edited the manuscript. This work was supported by National Institutes of Health Grants 2R01 NS039746 and 2R01 NS045191 from the National Institute of Neurological Disorders and Stroke and by Grant 2P01 AG022074 from the National Institute on Aging, the J. David Gladstone Institutes, and the Taube–Koret Center for Huntington Disease Research (to S.F.); a Milton Wexler Award and fellowship from the Hereditary Disease Foundation (to A.S.T.); and the National Institutes of Health-National Institute of General Medical Sciences University of California, San Francisco Medical Scientist Training Program, and a fellowship from the University of California, San Francisco Hillblom Center for the Biology of Aging (to J.M.). The animal care facility was partly supported by a National Institutes of Health Extramural Research Facilities Improvement Project (C06 RR018928).

1. Rubinsztein DC, Gestwicki JE, Murphy LO, Klionsky DJ (2007) Potential therapeutic applications of autophagy. *Nat Rev Drug Discov* 6:304–312.
2. Komatsu M, et al. (2006) Loss of autophagy in the central nervous system causes neurodegeneration in mice. *Nature* 441:880–884.
3. Mizushima N, Levine B, Cuervo AM, Klionsky DJ (2008) Autophagy fights disease through cellular self-digestion. *Nature* 451:1069–1075.
4. Webb JL, Ravikumar B, Atkins J, Skepper JN, Rubinsztein DC (2003) Alpha-Synuclein is degraded by both autophagy and the proteasome. *J Biol Chem* 278:25009–25013.
5. Fornai F, et al. (2008) Lithium delays progression of amyotrophic lateral sclerosis. *Proc Natl Acad Sci USA* 105:2052–2057.
6. Ravikumar B, et al. (2004) Inhibition of mTOR induces autophagy and reduces toxicity of polyglutamine expansions in fly and mouse models of Huntington disease. *Nat Genet* 36:585–595.
7. Nixon RA (2007) Autophagy, amyloidogenesis and Alzheimer disease. *J Cell Sci* 120: 4081–4091.
8. Fox JH, et al. (2010) The mTOR kinase inhibitor Everolimus decreases S6 kinase phosphorylation but fails to reduce mutant huntingtin levels in brain and is not neuroprotective in the R6/2 mouse model of Huntington's disease. *Mol Neurodegener* 5:26–38.
9. Sarkar S, et al. (2007) Small molecules enhance autophagy and reduce toxicity in Huntington's disease models. *Nat Chem Biol* 3:331–338.
10. Zhang L, et al. (2007) Small molecule regulators of autophagy identified by an image-based high-throughput screen. *Proc Natl Acad Sci USA* 104:19023–19028.
11. Williams A, et al. (2008) Novel targets for Huntington's disease in an mTOR-independent autophagy pathway. *Nat Chem Biol* 4:295–305.
12. Yue Z, Friedman L, Komatsu M, Tanaka K (2009) The cellular pathways of neuronal autophagy and their implication in neurodegenerative diseases. *Biochim Biophys Acta* 1793:1496–1507.
13. Mitra S, Tsvetkov AS, Finkbeiner S (2009) Single neuron ubiquitin-proteasome dynamics accompanying inclusion body formation in Huntington disease. *J Biol Chem* 284: 4398–4403.
14. Mitra S, Tsvetkov AS, Finkbeiner S (2009) Protein turnover and inclusion body formation. *Autophagy* 5:1037–1038.
15. Mizushima N, Yamamoto A, Matsui M, Yoshimori T, Ohsumi Y (2004) In vivo analysis of autophagy in response to nutrient starvation using transgenic mice expressing a fluorescent autophagosome marker. *Mol Biol Cell* 15:1101–1111.
16. Cota D, et al. (2006) Hypothalamic mTOR signaling regulates food intake. *Science* 312: 927–930.
17. Boland B, et al. (2008) Autophagy induction and autophagosome clearance in neurons: Relationship to autophagic pathology in Alzheimer's disease. *J Neurosci* 28: 6926–6937.
18. Wyttenbach A, Hands S, King MA, Lipkow K, Tolkovsky AM (2008) Amelioration of protein misfolding disease by rapamycin: Translation or autophagy? *Autophagy* 4:542–545.
19. King MA, et al. (2008) Rapamycin inhibits polyglutamine aggregation independently of autophagy by reducing protein synthesis. *Mol Pharmacol* 73:1052–1063.
20. Thimmaiah KN, et al. (2005) Identification of N10-substituted phenoxazines as potent and specific inhibitors of Akt signaling. *J Biol Chem* 280:31924–31935.
21. Klionsky DJ, et al. (2008) Guidelines for the use and interpretation of assays for monitoring autophagy in higher eukaryotes. *Autophagy* 4:151–175.
22. Mizushima N, Yoshimori T, Levine B (2010) Methods in mammalian autophagy research. *Cell* 140:313–326.
23. Bradley J, Carter SR, Rao VR, Wang J, Finkbeiner S (2006) Splice variants of the NR1 subunit differentially induce NMDA receptor-dependent gene expression. *J Neurosci* 26:1065–1076.
24. Yamamoto A, et al. (1998) Bafilomycin A1 prevents maturation of autophagic vacuoles by inhibiting fusion between autophagosomes and lysosomes in rat hepatoma cell line, H-4-II-E cells. *Cell Struct Funct* 23:33–42.
25. Fengsrud M, et al. (1995) Ultrastructural and immunocytochemical characterization of autophagic vacuoles in isolated hepatocytes: Effects of vinblastine and asparagine on vacuole distributions. *Exp Cell Res* 221:504–519.
26. Hariri M, et al. (2000) Biogenesis of multilamellar bodies via autophagy. *Mol Biol Cell* 11:255–268.
27. Arrasate M, Mitra S, Schweitzer ES, Segal MR, Finkbeiner S (2004) Inclusion body formation reduces levels of mutant huntingtin and the risk of neuronal death. *Nature* 431:805–810.
28. Arrasate M, Finkbeiner S (2005) Automated microscope system for determining factors that predict neuronal fate. *Proc Natl Acad Sci USA* 102:3840–3845.
29. Mangiarini L, et al. (1996) Exon 1 of the HD gene with an expanded CAG repeat is sufficient to cause a progressive neurological phenotype in transgenic mice. *Cell* 87: 493–506.
30. Barnett SF, et al. (2005) Identification and characterization of pleckstrin-homology-domain-dependent and isoenzyme-specific Akt inhibitors. *Biochem J* 385:399–408.
31. Barnum D, Greene J, Smellie A, Sprague P (1996) Identification of common functional configurations among molecules. *J Chem Inf Comput Sci* 36:563–571.
32. Rao VR, et al. (2006) AMPA receptors regulate transcription of the plasticity-related immediate-early gene Arc. *Nat Neurosci* 9:887–895.
33. Fung C, Lock R, Gao S, Salas E, Debnath J (2008) Induction of autophagy during extracellular matrix detachment promotes cell survival. *Mol Biol Cell* 19:797–806.